Extended Male Growth in a Fossil Hominin Species
Charles A. Lockwood, *et al.*
Science **318**, 1443 (2007);
DOI: 10.1126/science.1149211

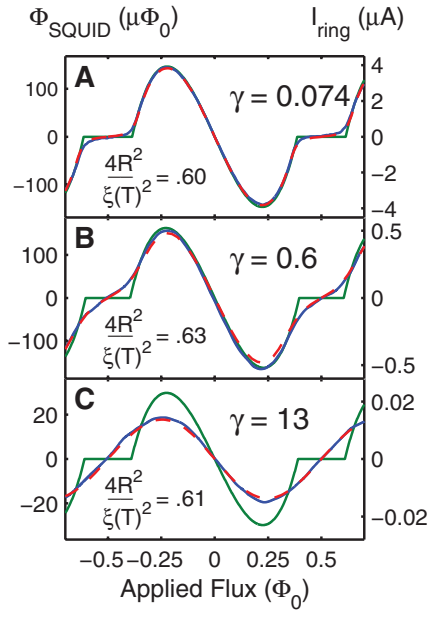

Fig. 4. Mean field theory (green), fluctuation theory (dashed red), and data (blue) for three rings with different γ parameters. The mean field response is derived from the fluctuation theory parameters for each ring at the given temperature. (**A**) $T = 1.20$ K. In small γ rings, the Little-Parks line shape is clearly observable. (**B**) $T = 1.25$ K. When $\gamma \approx 1$, the reduction of the response due to the Little-Parks effect is significantly suppressed. (**C**) $T = 1.25$ K. In large γ rings, the Little-Parks effect is completely washed out by fluctuations, which affect the responses at all flux values.

imation would predict a divergent susceptibility (Fig. 3A). By using Eq. 1 to define an effective superfluid density from the zero field response, $1/\lambda_{\mathrm{eff}}^2 = (\mu_0 L/wd)\partial I/\partial\Phi_a|_{\Phi_a=0}$, one can see (Fig. 3B) that fluctuations make the susceptibility deviate from the mean field response below $T_c(0)$, gradually smoothing the transition. Our parameterization of the theory shows that γ is the only sample-dependent parameter at $T = T_c(0)$. The temperature range where non-Gaussian fluctuations are important is typically parameterized through the Ginzburg parameter as $|T - T_c(\Phi_a)|/T_c(\Phi_a) < Gi$, where $|T - T_c(\Phi_a)|/E_c < \frac{T_c(\Phi_a)}{E_c} Gi \propto \sqrt{\gamma}$ (*13*). Inside this range, γ determines the magnitude of the response. Far above this range, Gaussian fluctuations dominate, and the susceptibility is a function of $|T - T_c(0)|/E_c \propto L^2/\xi^2$ alone.

The theory's dependence on γ allows us to state the criterion for the visibility of the Little-Parks effect in the context of fluctuations. The region that is shaded in green in Fig. 3C is above $T_c(\Phi_0/2)$ because $\xi(T) > 2R$. The susceptibility would be zero in this regime if fluctuation effects were not considered. When $\gamma \ll 1$, the distinct Little-Parks shape is visible in that the susceptibility is smaller at $\Phi_a = \Phi_0/2$ than at $\Phi_a = 0$. However, when $\gamma \gg 1$, the Little-Parks shape is entirely washed out by fluctuations (Fig. 4). For sufficiently large γ, the susceptibilities at $\Phi = 0$ and $\Phi_0/2$ are equal and opposite even below $T_c(\Phi_a = \Phi_0/2)$, so the response appears sinusoidal. This dependence on γ, rather than L and $\xi(T)$ alone, is the reason why the Little-Parks line shape does not occur in the ring shown in Figs. 2A and 4C.

Several factors contribute to the large fluctuation response near $\Phi_a = \Phi_0/2$ above $T_c(\Phi_a)$. First, the Gaussian fluctuations between $T_c(\Phi_a = 0)$ and $T_c(\Phi_a)$ have a large magnitude, which is due to the interplay between adjacent phase winding states. In small γ rings, the non-Gaussian fluctuation region in Fig. 3C is small. Thus, there is a large region where the magnitude of the persistent current near $\Phi_a = \Phi_0/2$ is strictly a function of $k_B[T - T_c(0)]/E_c$. In large γ rings, non-Gaussian fluctuations play an increased role in the phase diagram, and multiple phase winding modes need to be considered (*13*), indicating the importance of phase fluctuations. In all rings, nonhomogeneous wave functions may have a nonnegligible contribution to the final currents because of their vanishing energy cost near $T_c(\Phi_a)$. Small variations in width (SOM text) make nonhomogeneous wave functions more important (*14*) and would be important to include in an extended theory.

Fluctuation effects play a important role in 1D superconducting structures. Our analysis explicitly demonstrates how Gaussian and non-Gaussian fluctuations affect the persistent current in rings with various diameters and cross sections, as a function of applied magnetic flux. A single parameter, γ, characterizes the fluctuations for a given ratio of the temperature-dependent coherence length to the circumference. When γ is large, the signature of a Little-Parks flux-dependent $T_c(\Phi_a)$ is entirely washed out by fluctuations. When γ is small, the susceptibility in the non-Gaussian region near $T_c(\Phi_a)$ is enhanced, and Gaussian fluctuations are clearly visible between $T_c(\Phi_a)$ and $T_c(0)$ for $\Phi_a \approx \Phi_0/2$. This new framework for understanding Little-Parks fluctuations is supported by our data on fluctuation-induced currents in rings.

References and Notes

1. V. Emery, S. Kivelson, *Nature* **374**, 434 (1995).
2. J. M. Kosterlitz, D. J. Thouless, *J. Phys. C* **6**, 1181 (1973).
3. J. S. Langer, V. Ambegaokar, *Phys. Rev.* **164**, 498 (1967).
4. C. N. Lau, N. Markovic, M. Bockrath, A. Bezryadin, M. Tinkham, *Phys. Rev. Lett.* **87**, 217003 (2001).
5. F. von Oppen, E. K. Riedel, *Phys. Rev. B* **46**, 3203 (1992).
6. D. J. Scalapino, M. Sears, R. A. Ferrell, *Phys. Rev. B* **6**, 3409 (1972).
7. X. Zhang, J. C. Price, *Phys. Rev. B* **55**, 3128 (1997).
8. W. A. Little, R. D. Parks, *Phys. Rev. Lett.* **9**, 9 (1962).
9. Y. Liu *et al.*, *Science* **294**, 2332 (2001).
10. M. M. Rosario *et al.*, *Physica B* **329–333**, 1415 (2003).
11. M. Hayashi, H. Ebisawa, *Physica C* **352**, 191 (2001).
12. Materials and methods are available as supporting material on *Science* Online.
13. M. Daumens, C. Meyers, A. Buzdin, *Phys. Lett. A* **248**, 445 (1998).
14. J. Berger, J. Rubinstein, *Phys. Rev. Lett.* **75**, 320 (1995).

15. We acknowledge support from the Packard Foundation and NSF grants no. DMR-0507931, DMR-0216470, ECS-0210877, ECS-9731293, and PHY-0425897. We thank J. Price, Y. Imry, M. R. Beasley, Y. Oreg, and especially G. Schwiete for helpful discussions and A. Bachar for the illustration in Fig. 1B.

Supporting Online Material

www.sciencemag.org/cgi/content/full/318/5855/1440/DC1
Materials and Methods
SOM Text
Tables S1 and S2

3 August 2007; accepted 16 October 2007
10.1126/science.1148758

Extended Male Growth in a Fossil Hominin Species

Charles A. Lockwood,[1,2]* Colin G. Menter,[3] Jacopo Moggi-Cecchi,[2,4] Andre W. Keyser[2]

In primates that are highly sexually dimorphic, males often reach maturity later than females, and young adult males do not show the size, morphology, and coloration of mature males. Here we describe extended male development in a hominin species, *Paranthropus robustus*. Ranking a large sample of facial remains on the basis of dental wear stages reveals a difference in size and robusticity between young adult and old adult males. Combined with estimates of sexual dimorphism, this pattern suggests that male reproductive strategy focused on monopolizing groups of females, in a manner similar to that of silverback gorillas. However, males appear to have borne a substantial cost in the form of high rates of predation.

Sexual dimorphism is the only direct skeletal evidence available for reconstructing the evolution of human social behavior, and as such it is routinely analyzed and debated when seen in extinct hominin species (*1*–*6*). The expectation is that higher levels of sexual dimorphism correlate with higher levels of male-male competition and social systems in which males control mating access to multiple females (*7*). However, partly due to the limitations of small fossil samples, estimates of dimorphism have led to divergent inferences about social behavior in fossil hominins, ranging from monogamous to highly polygynous groups. Here we combine analysis of dimorphism with another aspect of life history—differences between males and females in the timing of maturity (*8*)—and use the results to reconstruct social behavior.

We focus on *Paranthropus robustus*, a South African robust australopithecine, because there are a large number of specimens available (35 were used in our study). This species is known primarily from the Swartkrans site, Kromdraai, and recent finds from Drimolen (*9*, *10*). The *P. robustus* deposits at these sites have been dated to 1.5 to 2.0 million years ago (*10*–*12*). In order to compare size to relative age among adults, we only considered individuals with (i) M3 erupted, (ii) sufficient parts of the face and mandible preserved to compare size, and (iii) postcanine teeth well enough preserved to determine age from the relative degree of tooth wear. This selection resulted in 19 specimens of the face or maxilla, 17 of which are from Swartkrans, and 1 each from Drimolen and Kromdraai. For mandibles, 16 specimens meet the criteria, of which 10 are from Swartkrans, 5 from Drimolen, and 1 from Kromdraai (Table 1). Because many specimens are fragmentary, we determined a nonparametric ranking of individuals based on overall size rather than a specific measurement (*13*). Age ranks were determined on the basis of tooth wear of the postcanine row, following generally accepted methods (*13*, *14*). The sample represents nearly every stage of dental wear from young adulthood to old age (*15*).

From this analysis, we infer that maximum (presumably male) size was greater among old adults than young adults (Fig. 1). Old adults in the higher size ranks also had the most well-developed morphology with respect to features diagnostic of the *P. robustus* face, such as the anterior pillars and maxillary trigon (*16*) (Fig. 2). Based on the ontogeny of sexual dimorphism in modern primates (*17*), we interpret this pattern as continued growth in males between early skeletal adulthood and full maturity. Minimum size, on the other hand, occurs throughout the age range. For example, SK 21 is the oldest specimen in the sample of maxillas, but also the smallest. Because small, relatively gracile individuals occur at every age, we conclude that females have reached full skeletal size by the time M3 has erupted or soon thereafter.

Extended male growth occurs in primates when male reproductive success is concentrated in a period of dominance resulting from intense male-male competition (*17*, *18*). Climbing the dominance hierarchy typically involves not only an increase in size but also changes in soft-tissue anatomy and, in some taxa, coloration (*18*). Bimaturism can be interpreted as part of a male strategy to delay competition with high-ranking males until the likelihood of success is greatest (*17*, *19*, *20*).

[1]Department of Anthropology, University College London, Gower Street, London WC1E 6BT, UK. [2]Institute for Human Evolution, University of the Witwatersrand, WITS 2050, Johannesburg, South Africa. [3]Department of Anthropology and Development Studies, University of Johannesburg, Post Office Box 524 Auckland Park, Johannesburg, South Africa. [4]Laboratori di Antropologia, Dipartimento di Biologia Animale e Genetica, and Museo di Storia Naturale, Università di Firenze, 12 via del Proconsolo, 50122 Firenze, Italy.

*To whom correspondence should be addressed. E-mail: c.lockwood@ucl.ac.uk

In primates showing bimaturism, sexual dimorphism in the eruption of the last permanent tooth (M3 or the canine) is clearly less than the differences in reaching maturity in body mass. For example, male and female gorillas complete dental emergence at similar times (*21*, *22*), but gorilla male growth in body mass continues for years (*17*), and male gorillas do not become socially adult until as much as 5 or 6 years after females (*23*). In a more extreme case, eruption of the permanent teeth in mandrills is completed in males before females (*24*), but males continue to grow in body mass and body length for several years (*25*). Differences between dentally mature males and physically or socially mature males are thus well-recognized in modern primates.

Understanding sexual dimorphism in *P. robustus* has been aided by the discovery of DNH 7, a complete skull from Drimolen (*9*, *10*). It is substantially smaller than the well-preserved skulls of *P. robustus* from Swartkrans (such as SK 12, SK 46, SK 48, and SK 83) and Kromdraai (TM 1517) (table S1). Differences between DNH 7 and larger individuals are consistent with those expected between females and males. For example, the larger individuals have sagittal crests reaching onto the frontal bone, as well as deeply projecting mastoid processes, whereas DNH 7 lacks a sagittal crest and has reduced mastoid regions. The degree of size difference between DNH 7 and larger, presumably male specimens can be explained by a gorillalike level of sexual dimorphism but not the lower levels of dimorphism seen in chimpanzees and modern humans (supporting online material). Furthermore, it is unlikely that any of the other relatively complete skulls are female. In comparison to extant hominoids, the difference between even the smallest of the previously known crania (TM 1517) and DNH 7 is statistically greater than would be expected within the range of variation of females (supporting online text and table S2). The size of DNH 7, in combination with an understanding of male life history, helps resolve the sex of specimens such as SK 48 and TM 1517 (*26*, *27*). The two latter specimens are best regarded as young adult males.

A bias toward males among the well-preserved skulls is also reflected in the sample of maxillas as a whole (*28*). Specimens such as SK 21, SK 821, and SKW 8 are similar in size and proportions to DNH 7 and are probably females (these are size ranks 1 and 2 in Fig. 1), whereas all other specimens show male size and/or morphology (supporting online material). We conclude that the maxillofacial specimens represent 4 females and 15 males overall, and 3 females and 14 males for the Swartkrans sample only. This distribution deviates significantly from random sampling of an unbiased population (using a two-tailed binomial test and assuming a 50:50 ratio, $P = 0.0192$ for the overall sample and $P = 0.0127$ for Swartkrans).

An abundance of males is perhaps not surprising in a fossil sample that resulted largely from predation. Direct evidence of carnivore activity is present on several hominin specimens at Swartkrans, and member 1 of this site is among the most definitive examples of a predator-accumulated assemblage of hominins (*27*, *29*). In dimorphic primates, nondominant males spend more time alone, on the periphery of a social group, or in small all-male bands (*30*). Solitary behavior places males at risk (*31*, *32*). For example, when male baboons disperse, they suffer a mortality rate at least three times as great as that of group-living males or females (*32*). This

Table 1. Ranking of size and age (displayed in Fig. 1). Swartkrans member 1 (M1) includes all specimens from deposits referred to as the lower bank and the hanging remnant [see (*12*) for explanation].

Maxillas				Mandibles			
Specimen	Provenience	Age	Size	Specimen	Provenience	Age	Size
SKW 11	Swartkrans M1	1	3	TM 1517	Kromdraai B	1	1
TM 1517	Kromdraai B	1	4	SKW 5	Swartkrans M1	1	2
SK 48	Swartkrans M1	1	6	DNH 8	Drimolen	1	4
SK 49	Swartkrans M1	1	6	SKX 5013	Swartkrans M2	2	1
SK 821	Swartkrans M1	2	2	SK 23	Swartkrans M1	2	2
SK 65	Swartkrans M1	2	4	SK 34	Swartkrans M1	2	4
SK 57	Swartkrans M1	2	7	SK 858	Swartkrans M1	2	5
SKW 29	Swartkrans M1	2	7	DNH 7	Drimolen	3	3
DNH 7	Drimolen	3	1	DNH 21	Drimolen	4	2
SK 11	Swartkrans M1	4	5	SK 844	Swartkrans M1	4	3
SK 826/877	Swartkrans M1	4	8	SK 74A	Swartkrans M1	5	3
SKW 12	Swartkrans M1	4	9	DNH 19	Drimolen	5	6
SKW 8	Swartkrans M1	5	2	SK 1586	Swartkrans M1	5	6
SK 46	Swartkrans M1	5	5	SK 81	Swartkrans M1	5	6
SK 79	Swartkrans M1	5	6	DNH 6	Drimolen	6	5
SK 1512	Swartkrans M1	5	8	SK 12	Swartkrans M1	6	7
SK 83	Swartkrans M1	6	7				
SK 12	Swartkrans M1	6	8				
SK 21	Swartkrans M1	7	1				

degree of difference in mortality matches the male bias at Swartkrans. Females were apparently more shielded from predation. Putting this observation together with the conclusions about bimaturism and sexual dimorphism, we infer that the distribution of food sources allowed stable groups of *P. robustus* females to form in response to predation pressure, and males in turn sought to monopolize reproductive access to these groups (*33*). If females emigrated from their natal groups, then it is likely that they spent little time alone and transferred directly to a male or an established group [as occurs in gorillas (*30*, *34*)].

The *P. robustus* pattern contrasts with that of some other australopithecine collections. For example, the sample of *Australopithecus africanus* is either biased toward females or shows no bias (*4*). The *A. africanus* accumulation from Sterkfontein member 4 may also be the product of predator behavior, but this conclusion is less certain than for the Swartkrans sample (*27*, *35*). If both Swartkrans member 1 and Sterkfontein member 4 hominin collections are largely attributable to carnivore activity, the difference in sex bias raises the possibility that *P. robustus* and *A. africanus* differed in social structure.

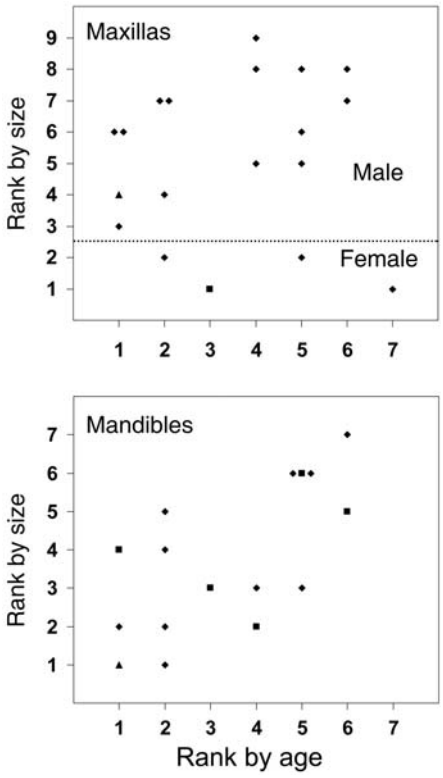

Fig. 1. Comparison of size ranks to age ranks for adult maxillofacial and mandibular specimens (Swartkrans, diamonds; Drimolen, squares; Kromdraai, triangles). Table 1 lists the specimens used here. The lowest age rank contains individuals with M3 recently erupted. The largest individuals are more advanced in age, showing at least some dentine exposure on M2. When a randomization test of correlation coefficients is used, age and size are significantly correlated among the male maxillofacial specimens (r = 0.52; P = 0.027, one-tailed test, 5000 permutations).

References and Notes

1. J. M. Plavcan, C. P. van Schaik, *J. Hum. Evol.* **32**, 345 (1997).
2. H. M. McHenry, *J. Hum. Evol.* **27**, 77 (1994).
3. R. A. Foley, P. C. Lee, *Science* **243**, 901 (1989).
4. C. A. Lockwood, *Am. J. Phys. Anthropol.* **108**, 97 (1999).
5. P. L. Reno, R. S. Meindl, M. A. McCollum, C. O. Lovejoy, *Proc. Natl. Acad. Sci. U.S.A.* **100**, 9404 (2003).
6. We refer to differences in skull size and morphology between males and females, which have been shown to correlate with sexual dimorphism in body mass (*36*).
7. J. M. Plavcan, *Yrbk. Phys. Anthropol.* **116**, 25 (2001).
8. Bimaturism, defined as sex differences in the timing of cessation of growth (*17*).
9. A. W. Keyser, *S. Afr. J. Sci.* **96**, 189 (2000).
10. A. W. Keyser, C. G. Menter, J. Moggi-Cecchi, T. R. Pickering, L. R. Berger, *S. Afr. J. Sci.* **96**, 193 (2000).
11. E. S. Vrba, in *Hominid Evolution: Past, Present and Future*, P. V. Tobias, Ed. (Liss, New York, 1985), pp. 195–200.
12. C. K. Brain, in *Swartkrans: A Cave's Chronicle of Early Man*, C. K. Brain, Ed. (Monograph 8, Transvaal Museum, Pretoria, South Africa, 1993), pp. 23–33.
13. Further information on materials and methods is available as supporting material on *Science* Online.
14. S. Hillson, *Teeth* (Cambridge Univ. Press, New York, ed. 2, 2005).
15. In specimens with M3 recently erupted (such as SK 48, TM 1517, and DNH 8), small dentine islands are present on the M1s. Given schedules of dental development in *P. robustus* [M1 erupted at 3 years and M3 erupted at approximately 9 years (*37*)], this implies that tooth wear on M1 began to expose dentine after 6 years. M2 erupted approximately halfway between M1 and M3. If it underwent comparable amounts of wear to M1, then individuals of age rank 4 (which have exposed dentine on M2) are at least 3 years older than those in age rank 1.
16. Y. Rak, *The Australopithecine Face* (Academic Press, New York, 1983).
17. S. R. Leigh, *Am. J. Phys. Anthropol.* **97**, 339 (1995).
18. J. M. Setchell, P. C. Lee, in *Sexual Selection in Primates*, P. M. Kappeler, C. P. van Schaik, Eds. (Cambridge Univ. Press, Cambridge, 2004), pp. 175–195.
19. P. J. Jarman, *Biol. Rev.* **58**, 485 (1983).
20. C. H. Janson, C. P. van Schaik, in *Juvenile Primates: Life History, Development, and Behavior*, M. E. Pereira, L. A. Fairbanks, Eds. (Oxford Univ. Press, Oxford, 1993), pp. 57–74.
21. M. C. Dean, B. A. Wood, *Folia Primatol. (Basel)* **36**, 111 (1981).
22. B. H. Smith, T. L. Crummett, K. L. Brandt, *Yrbk. Phys. Anthropol.* **37**, 177 (1994).
23. D. P. Watts, A. E. Pusey, in *Juvenile Primates: Life History, Development, and Behavior*, M. E. Pereira, L. A. Fairbanks, Eds. (Oxford Univ. Press, Oxford, 1993), pp. 148–172.
24. J. M. Setchell, E. J. Wickings, *Folia Primatol. (Basel)* **75**, 121 (2004).
25. J. M. Setchell, E. J. Wickings, L. A. Knapp, *Am. J. Phys. Anthropol.* **131**, 498 (2006).
26. M. H. Wolpoff, in *Paleoanthropology, Morphology and Paleoecology*, R. Tuttle, Ed. (Mouton, The Hague, Netherlands, 1975), pp. 245–284.
27. C. K. Brain, *The Hunters or the Hunted? An Introduction to African Cave Taphonomy* (Univ. of Chicago Press, Chicago, 1981).
28. We do not assign sexes to mandibles, because they are generally more fragmentary and there is greater overlap in male and female mandible size in sexually dimorphic hominoids.
29. K. J. Carlson, T. R. Pickering, *J. Hum. Evol.* **44**, 431 (2003).
30. A. Pusey, C. Packer, in *Primate Societies*, B .B. Smuts, D. L. Cheney, R. M. Seyfarth, R. W. Wrangham, T. T. Struhsaker, Eds. (Univ. of Chicago Press, Chicago, 1987), pp. 250–266.
31. G. Cowlishaw, *Behaviour* **131**, 293 (1994).
32. S. C. Alberts, J. Altmann, *Am. Nat.* **145**, 279 (1995).
33. E. H. M. Sterck, D. P. Watts, C. P. van Schaik, *Behav. Ecol. Sociobiol.* **41**, 291 (1997).
34. E. J. Stokes, R. J. Parnell, C. Olejniczak, *Behav. Ecol. Sociobiol.* **54**, 329 (2003).
35. T. R. Pickering, R. J. Clarke, J. Moggi-Cecchi, *Am. J. Phys. Anthropol.* **125**, 1 (2004).
36. J. M. Plavcan, *J. Hum. Evol.* **42**, 579 (2002).
37. M. C. Dean, in *Evolutionary History of the "Robust" Australopithecines*, F. E. Grine, Ed. (Aldine de Gruyter, New York, 1988), pp. 43–53.

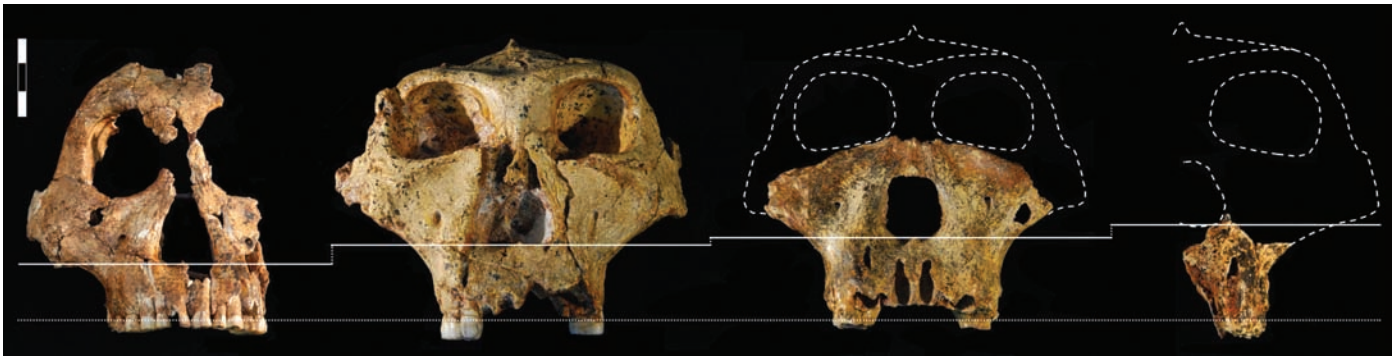

Fig. 2. Size and morphological comparisons among DNH 7, SK 48, SK 12, and SKW 12 (from left to right). They are aligned approximately on the cementum-enamel junction of the molars, indicated by the lower line. Upper lines indicate the level of the inferior nasal margin as a general size comparison. DNH 7 is the most well-preserved female specimen of *P. robustus* (the mandible and cranial vault are not shown here). SK 48 is one of the largest young adult males. SK 12 and SKW 12 are older adult males. Drawings for SK 12 and SKW 12 are for schematic purposes only. Scale bar, 3 cm.

38. This work stems from excavations at Drimolen, supported by grants from the L. S. B. Leakey Foundation and the Department of Science and Technology in South Africa. Further financial support was provided to C.A.L. by the Royal Society, UK. A.W.K. and C.G.M. thank D. and J. Smith, on whose property Drimolen is situated, for permission to conduct the excavation and for their assistance. J.M.C. received support from the Italian Ministry of Foreign Affairs (Direzione Generale per la Promozione e la Cooperazione Culturale, ufficio V, Archaeology), and the Italian Embassy and Italian Cultural Institute in Pretoria. We also thank D. Shima and D. Kekane for their continued help with the Drimolen excavation; B. Zipfel and S. Potze for assistance with specimens; and Z. Alemseged, B. Bradley, C. Dean, W. Kimbel, S. Leigh, M. Plavcan, J. Setchell, J. Scott, and F. Spoor for discussion and comments.

Supporting Online Material
www.sciencemag.org/cgi/content/full/318/5855/1443/DC1
SOM Text
Tables S1 and S2
References

14 August 2007; accepted 24 October 2007
10.1126/science.1149211

Boron-Toxicity Tolerance in Barley Arising from Efflux Transporter Amplification

Tim Sutton,* Ute Baumann, Julie Hayes, Nicholas C. Collins, Bu-Jun Shi, Thorsten Schnurbusch, Alison Hay, Gwenda Mayo, Margaret Pallotta, Mark Tester, Peter Langridge

Both limiting and toxic soil concentrations of the essential micronutrient boron represent major limitations to crop production worldwide. We identified *Bot1*, a *BOR1* ortholog, as the gene responsible for the superior boron-toxicity tolerance of the Algerian barley landrace Sahara 3771 (Sahara). *Bot1* was located at the tolerance locus by high-resolution mapping. Compared to intolerant genotypes, Sahara contains about four times as many *Bot1* gene copies, produces substantially more *Bot1* transcript, and encodes a Bot1 protein with a higher capacity to provide tolerance in yeast. *Bot1* transcript levels identified in barley tissues are consistent with a role in limiting the net entry of boron into the root and in the disposal of boron from leaves via hydathode guttation.

Of all plant nutrient elements, boron has the narrowest range between deficient and toxic soil solution concentration (*1*), and both boron deficiency and toxicity severely limit crop production worldwide (*2*, *3*). Toxicity is more difficult to manage agronomically and is best dealt with by using boron-tolerant varieties. Genetic variation for boron-toxicity tolerance is known for a number of crop plant species. Tolerance is most commonly associated with the ability to maintain low boron concentrations in the shoot (*4*–*6*). In barley (*Hordeum vulgare*), the non-agronomic but highly boron-tolerant Algerian landrace Sahara 3771 (Sahara) was identified as a potential source of tolerance for variety improvement (*4*, *7*). In a cross between Sahara and the boron-intolerant Australian malting variety Clipper, several quantitative trait loci (QTL) controlling tolerance were identified (*8*). The major locus on chromosome 4H affects leaf symptom expression (Fig. 1A), boron accumulation (Fig. 1B), root length response, and dry matter production under boron-toxic conditions (*8*). The ability of Sahara to maintain lower shoot boron accumulation is at least partially due to a mechanism of active boron efflux from the root (*9*).

We followed a map-based approach to isolate the 4H boron-tolerance gene. Using a population representing 6720 meioses and gene colinearity with the syntenic region on rice chromosome 3 to generate markers, we delimited the tolerance locus to a 0.15-centimorgan interval between markers *xBM178* and *xBM162* (Fig. 2A and fig. S1) (*10*). The corresponding 11.2-kb interval in rice contains two intact copies and one 3′-truncated version of a gene showing similarity to a family of adenosine monophosphate (AMP)–dependent synthetases and ligases and no other predicted gene. Barley expressed sequence tags (ESTs) most closely matching one of the intact copies were used to derive the marker *xBM160*, which cosegregated with the tolerance locus.

In a parallel approach, we also mapped several candidate genes in barley. These were barley genes showing similarity to the *Arabidopsis* NIP5;1 major intrinsic protein (*11*) and the *Arabidopsis* BOR1 efflux transporter that is related to bicarbonate transporters in animals (*12*, *13*). Both *Arabidopsis* genes are required for healthy growth under conditions of low boron supply. However, in plants the genes involved in boron-toxicity tolerance may be related to those shown to function in boron efficiency. Comparisons of barley ESTs revealed four *BOR1* (At2g47160.1)–related genes. Mapping localized one of the barley genes (*Bot1*) to the region of the boron-tolerance QTL on 4H (*8*). Subsequently, a marker developed from the 3′ end of *Bot1* was found to cosegregate perfectly with the tolerance locus in our high-resolution mapping population (Fig. 2A), strongly suggesting that *Bot1* encodes the boron tolerance from the 4H locus. Although barley/rice gene colinearity was found to be high in the region (Fig. 2A), the corresponding interval on rice chromosome 3 lacks a *BOR1* ortholog, and the rice gene most closely resembling *Bot1* (Os01g08040) (Fig. 2B) resides on chromosome 1.

Southern hybridization with the use of a Clipper derived *Bot1* probe gave a stronger signal in Sahara than in Clipper and other boron-intolerant genotypes, indicating the occurrence of additional *Bot1* copies in Sahara (fig. S2). A number of restriction enzyme digests revealed hybridizing Sahara fragments of mostly a single size (e.g.,

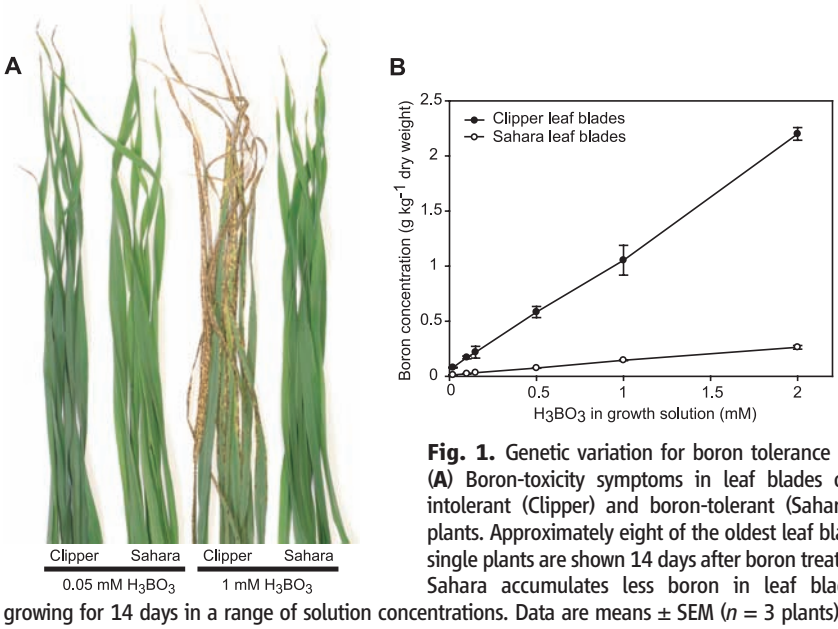

Fig. 1. Genetic variation for boron tolerance in barley. (**A**) Boron-toxicity symptoms in leaf blades of boron-intolerant (Clipper) and boron-tolerant (Sahara) barley plants. Approximately eight of the oldest leaf blades from single plants are shown 14 days after boron treatment. (**B**) Sahara accumulates less boron in leaf blades after growing for 14 days in a range of solution concentrations. Data are means ± SEM (n = 3 plants).

Australian Centre for Plant Functional Genomics, School of Agriculture, Food and Wine, University of Adelaide, Waite Campus, Private Mail Bag 1, Glen Osmond, South Australia 5064, Australia.

*To whom correspondence should be addressed. E-mail: tim.sutton@acpfg.com.au